ISSN (Print) 1226-1750
ISSN (Online) 2233-6656
Journal of Magnetics 21(4), 586-592 (2016) https://doi.org/10.4283/JMAG.2016.21.4.586

Design Optimization of CRDM Motor Housing

Jae Seon Lee*, Gyu Mahn Lee, and Jong Wook Kim

Korea Atomic Energy Research Institute, Daejeon 34057, Republic of Korea

(Received 2 November 2016, Received in final form 13 December 2016, Accepted 14 December 2016)

The magnetic-jack type CRDM withdraws or inserts a control rod assembly from/to the reactor core to control the core reactivity. The CRDM housings form not only the path of the electromagnetic field but also the pressure boundary of a nuclear reactor, and a periodic in-service inspection should be carried out if there are welded or flange jointed parts on the pressure boundary. The in-service inspection is a time-consuming process during the reactor refueling, and moreover it is difficult to perform the inspection over the reactor head. A magnetic motor housing is applied for the current SMART CRDM and has several welding joints, however a nonmagnetic motor housing with fewer or no welding joints may improve the operational efficiency of the nuclear reactor by avoiding or simplifying the in-service inspection process. Prior to the development, the magnetic field transfer efficiency of the nonmagnetic housing was required to be assessed. It was verified and optimized by the electromagnetic analysis of the lifting force estimation. Magnetic flux rings were adopted to improve the efficiency. In this paper, the design and optimization process of a nonmagnetic motor housing with the magnetic flux rings for the SMART CRDM are introduced and the analyses results are discussed.

Keywords : control rod drive mechanism, magnetic-jack type, flux ring, pressure housing

1. Introduction

The magnetic-jack type control rod drive mechanism (CRDM) withdraws or inserts a control rod assembly from/to the reactor core when shaped electrical pulses are received by the operating coils, and the reactivity of the reactor core is controlled as intended. SMART, which obtained standard design approval from the Nuclear Safety and Security Commission of Korea in 2012 for the first time as a small and medium-sized nuclear power reactor, has the magnetic jack type CRDMs. CRDM coils create magnetic fields around a motor assembly, and generated attraction between magnetic components makes the latches engage with or lift up the drive shaft connected with a control rod assembly. A drive shaft and control rod assembly drops by gravity. Reference [1] described the operational concept of a magnetic-jack type CRDM. The configuration of the SMART CRDM is shown in Figure 1.

The motor housing of the current SMART CRDM consists of a main body, which is made of magnetic stainless steel (AISI type 403 modified), and two ends, which are made of nonmagnetic stainless steel. The lower and upper ends are bolted and hermitically sealed by a canopy seal welding to a CRDM nozzle and a nonmagnetic upper pressure housing, respectively, which provides a path for a drive shaft through a reactor head. On the other hand, the AP1000 [2] of Westinghouse Electric Co. and the APWR [3] of Mitsubishi Heavy Industries have adopted

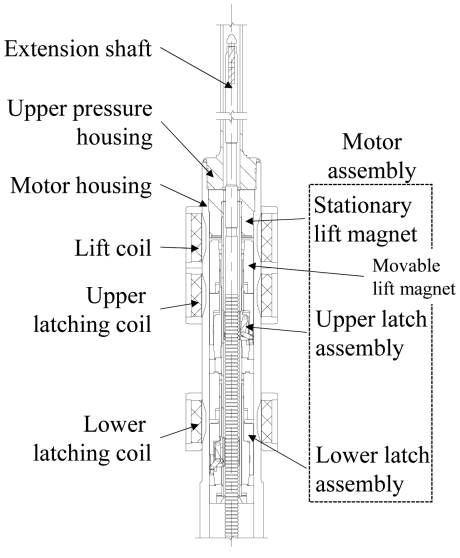

Fig. 1. SMART CRDM configuration.

*Corresponding author: Tel: +82-42-868-2826
Fax: +82-42-868-8188, e-mail: leejs@kaeri.re.kr

simple full-penetration welding, and EPR [4] of AREVA has adopted a flange joint. They accept a nonmagnetic motor housing.

The CRDM housings and CRDM nozzle form a primary pressure boundary of a nuclear reactor, and a periodic in-service inspection should be carried out according to references [5] and [6] for any types of pressure boundary if there are welded or flange jointed parts. A CRDM is located above the reactor head where complicated piping lines and a thermal insulator are installed. Therefore, it is very difficult to inspect the integrity of a pressure boundary. Several inspection methods have been proposed, for example, references [7] and [8]. If a CRDM nozzle and a motor housing become a single part, it may be exempt from in-service inspection, and the operational efficiency and integrity of a nuclear reactor will be enhanced.

Pressurized water reactor components may suffer from stress corrosion cracking (SCC). A CRDM nozzle is known as the vulnerable part to SCC, and Inconel alloy 690 (Alloy 690) is considered the most resistant to SCC thus far [9]. Therefore, it has been adopted as a CRDM nozzle material for almost every commercial nuclear reactor, along with SMART. A motor housing should be made of nonmagnetic Alloy 690 to become a single part with a CRDM nozzle. Even if a CRDM nozzle and a motor housing are made of different nonmagnetic materials, it is possible to reduce a welding joint by applying the same material for the upper pressure housing and the motor housing.

In this paper, the design and optimization process of the flux rings for a nonmagnetic motor housing of the SMART CRDM are introduced and the analysis results are discussed.

2. Analytical Approaching

Estimation of the CRDM lift force through a finite element electromagnetic analysis, for example, an APR+ CEDM coil assembly development [10, 11] and APR+ CEDM (Control Element Drive Mechanism) experiment and analytic verification [12], was proved to be reliable and proper for the design optimization of a CRDM drive system. Based on previous research and similar design concept [2, 3], the lift force of a newly designed SMART CRDM with a nonmagnetic motor housing and flux rings was estimated through a finite element electromagnetic analysis, and the optimal design of the housing and flux rings was proposed. The CRDM lift force is the attraction between a stationary and a movable lift magnet of an upper latch assembly when a lift coil is activated and then these parts are magnetized. This is the maximum vertical force from the latches to lift a drive shaft and control rod assembly 10 mm upward. The latching force, which is an attraction for the latches to maintain engagement with a drive shaft, is also estimated.

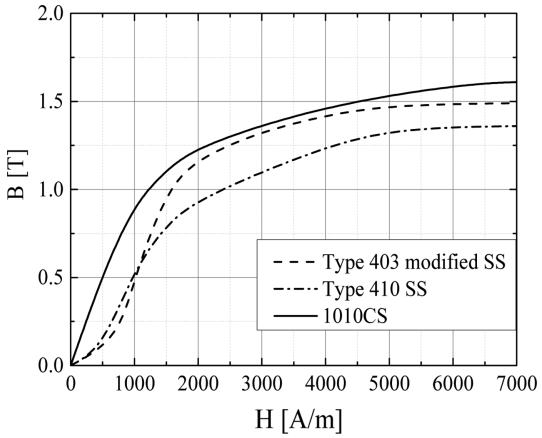

Fig. 2. Magnetic properties.

Table 1. Pressure housing material.

Material	Young's Modulus [MPa]	Stress intensity [MPa @350°C]
Type 403	2.01×10^5	145 (Annealed)
Alloy 690	2.09×10^5	161

2.1. Material properties

The magnetic properties of a 1010CS (coil housing), Type 410 Stainless steel (motor assembly parts), and AISI type 403 modified Stainless steel (motor housing) are summarized in Figure 2.

The mechanical properties of AISI type 403 modified stainless steel and Alloy 690 are compared in Table 1. Alloy 690 has equivalent or slightly higher stress intensity, and thus it seems that the minimum wall thickness of a motor housing does not need to be modified at this stage.

2.2. Current design review

The first step is to develop the analysis model and set the reference point by estimating the lifting force from the current housing design. A 2-D axisymmetric model for the CRDM was developed using ANSYS Maxwell [13]. At the beginning moment of the 10 mm lift of a drive shaft, the upper latching coil is on and the lower latching coil is off. Then, the lift coil is activated, and the upper latch assembly and the stationary lift magnet are magnetized. Attraction between them makes the latches lift the drive shaft, whose tooth is seated on the latches. When the attraction is greater than the load on the latches,

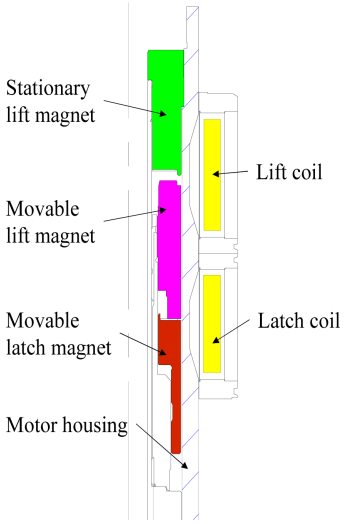

Fig. 3. (Color online) Analysis model for the SMART CRDM with a magnetic motor housing.

the drive shaft can be lifted. The load includes the weight of the drive shaft, control rod assembly, and spring restoration force between the upper latch assembly and the stationary lift magnet.

To apply this condition to the analysis model, the system was modeled with a closed latching gap in the upper latch assembly and the open latching gap in the lower latch assembly. The analysis model except the lower latch assembly is shown in Figure 3.

The magnetomotive forces (MMFs) on the lift and latching coils are the same as the SMART CRDM operating condition (on the lift coil, 15,000 A·turn, and on the latching coil, 5,100 A·turn for this study).

The lift force was estimated to be 4,100 N, and the flux lines and magnetic flux density distribution are shown in Figure 4. The figure shows that a magnetic field is formed in the motor housing and saturated at the neck, and is well formed along the movable magnet and stationary magnet for magnetizing them.

2.3. Design proposal

In the case of adopting a nonmagnetic motor housing, this diminishes the magnetic field transfer efficiency from the coils. Flux rings, which are magnetic, may be adopted to increase the transfer efficiency. The inside diameter of the motor housing and the minimum wall thickness are assumed to be 125 mm and 9 mm, respectively. The new configuration is shown in Figure 5. The same material as the coil housing is assumed to be applied. The outside diameter is the same as the maximum outside diameter of the motor housing, and the inside diameter is the same as the neck outside diameter of the motor housing. The MMFs are assumed to be the same as the current operating condition.

The design variables of the motor housing and flux ring may be the dimensions of three flux rings and their arrangement. Because there are so many design variables to be optimized, design optimization may be a time-consuming effort. Thus, some of the variables were excluded as follows:

Because the lower latching coil is not activated, the design effect of Flux ring C on the development of the electromagnetic field in the motor housing is assumed to be ignorant at this stage. Thus, Flux ring C was assumed to be the same as Flux ring B. In addition, the thicknesses

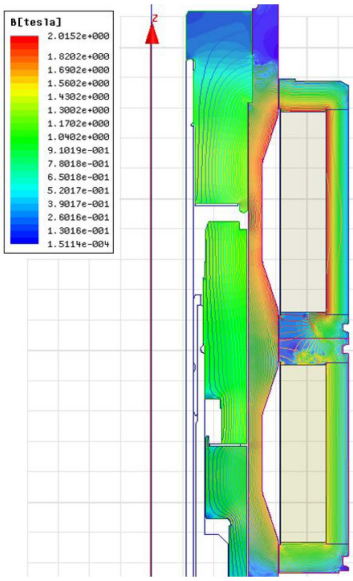

Fig. 4. (Color online) Flux lines and magnetic flux density distribution.

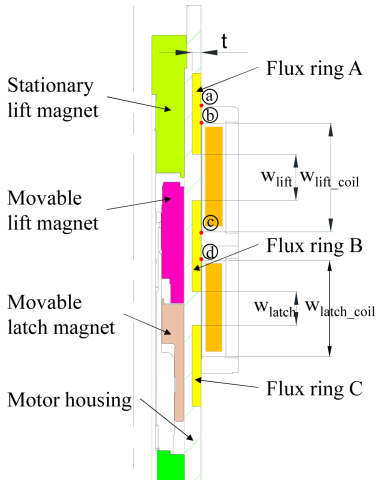

Fig. 5. (Color online) Analysis model for a nonmagnetic motor housing and flux rings.

of the flux rings were assumed to be the same. The width center of the flux ring window was assumed to be aligned with the width center of the coil housing.

Then, the following two parameters remained as design variables:

– Ratio of the flux ring window to the coil housing width (the window ratio):

$$\left(\frac{w_{lift}}{w_{lift\ coil}}, \frac{w_{latch}}{w_{latch\ coil}}\right)$$

2.4. Design optimization

To simplify the process, a three-step optimization process was proposed. The optimization steps are summarized as follows:

Step 1: Estimate the lift force with the increasing length of flux rings 5 mm uniformly both ways from the ends of the coil housing (i.e., ⓑ and ⓒ in Figure 5 for the lift coil housing). Search for the optimal lift window ratio.

Step 2: Estimate the lift force with the optimal lift window ratio from Step 1 and the varying latching window ratio. Search for the optimal latching window ratio.

Step 3: Estimate the lift force with the optimal latching window ratio from Step 2 and the varying lift window ratio. Search for the optimal lift window ratio.

The optimization step can be finalized until the results from Step 3 coincide with the results from Step 2. If not, the optimization step will continue from Step 2 with the results from Step 3.

1) The first optimization step

The first step is to seek the temporary optimal points. The initial optimal lift window ratio was searched with varying lift and latching flux ring lengths. The distance from ⓐ in Figure 5 to the uppermost face of Flux ring A is assumed to be the same as the distance from ⓑ to the lowermost face. The analyses results are shown in Table 2, and the lift and latching forces (F_{lift}, F_{latch}) are summarized in Figure 6. The lift and latching forces in the graph are according to the lift window ratio and latching window ratio, respectively.

Seven cases were considered, and analysis pairs for Flux rings A and B were marked as Case 0 to Case 6. Case 0 is for the single piece flux ring (i.e., zero window ratio), and the window ratio increases along with the cases. The flux lines and magnetic flux density distribution are shown in Figure 7 for the representative cases, Case 0, Case 1, and Case 3. If the flux ring is a single piece, the majority of magnetic flux flows through the flux ring, and the remaining flux flows through the stationary lift magnet and movable lift magnet owing to the difference in magnetic resistance. This produces low lift and latching forces.

On the contrary, if a flux ring window exists, a substantial portion of magnetic flux flows through the stationary

Table 2. Analysis results from the first optimization step.

Case	w_{lift} / w_{lift} [%]	w_{latch} / $w_{latch\ cc}$ [%]	F_{lift} [N]	F_{latch} [N]
0	0	0	2888.6	2339.6
1	11.8	0.83	3724.5	2415.8
2	19.1	9.1	3990	3194.4
3	26.5	17.4	4095.8	3238.9
4	33.8	25.6	4063.7	3113
5	41.2	33.9	3960.3	2983.1
6	55.9	50.4	3670.6	2736.4

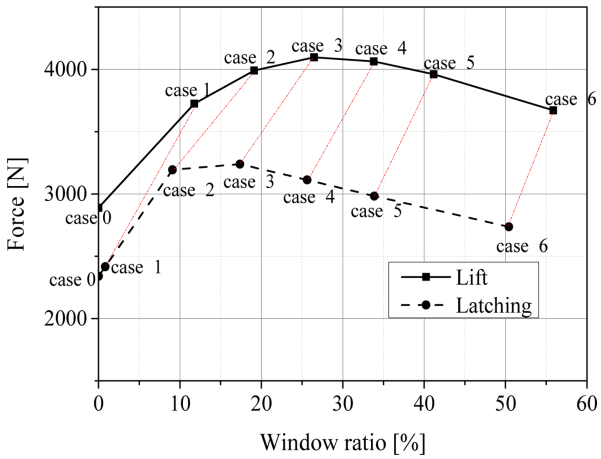

Fig. 6. (Color online) Lift and latching forces from the first optimization step.

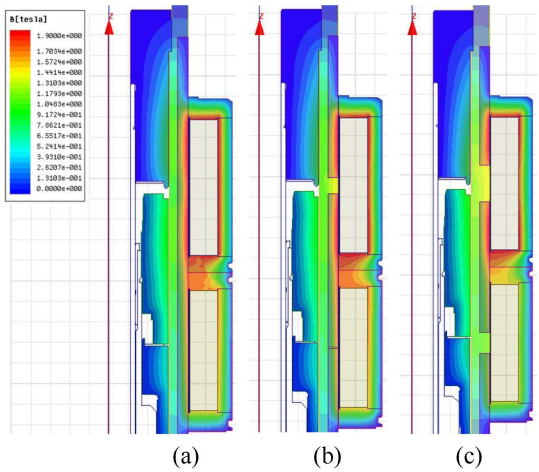

Fig. 7. (Color online) Flux lines and magnetic flux density distribution for the analysis cases 0, 1, and 3 from the first optimization step.

Table 3. Analysis results from the second optimization step.

Case	w_{lift} / $w_{lift\ coil}$ [%]	w_{latch} / $w_{latch\ coil}$ [%]	F_{lift} [N]	F_{latch} [N]
1	26.5	1	4097.3	2419.0
2		5	4089.2	2986.4
3		10	4086.7	3208.4
4		15	4087.0	3254.4
5		20	4085.5	3199.9
6		25	4085.6	3124.5
7		30	4085.4	3041.1

Table 4. Analysis results from the third optimization step.

Case	w_{lift} / $w_{lift\ coil}$ [%]	w_{latch} / $w_{latch\ coil}$ [%]	F_{lift} [N]	F_{latch} [N]
1	10	16.5	3602.7	3263.2
2	15		3857.1	3258.6
3	20		4012.3	3254.3
4	25		4081.5	3246.8
5	30		4082.0	3243.1
6	35		4043.4	3236.6
7	40		3976.0	3234.7

lift magnet and movable lift magnet and enlarges the lift and latching forces. However, too large a flux ring window produces a lower lift and latching forces, as shown for Cases 5 or 6. In addition, this shows that there may be a different optimal design range for each flux ring window.

2) The second optimization step

CRDM lift and latching forces using the optimized lift window ratio from Step 1 and the varying latching window ratio were estimated from Step 2. The lift window ratio was fixed as 26.5 %, and the latching window ratio varied from 1 to 30 %. The distance from ⓒ in Figure 5 to the uppermost face of Flux ring B did not change through this process, but the distance from ⓓ to the lowermost face of Flux ring B did change.

The analysis conditions and results are summarized in Table 3, and the estimated lift and latching forces are compared in Figure 8 according to the varying latching window ratio.

The results show that the lift force is slightly influenced by the latching window ratio variation, and the maximum latching force is generated at around 15 % of the latching window ratio. This tendency coincides with the results from Step 1.

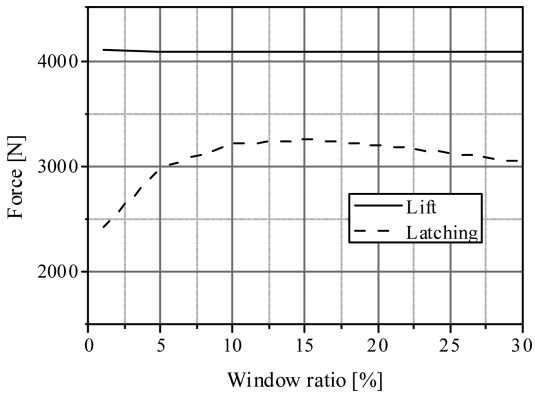

Fig. 8. Lift and latching forces from the second optimization step.

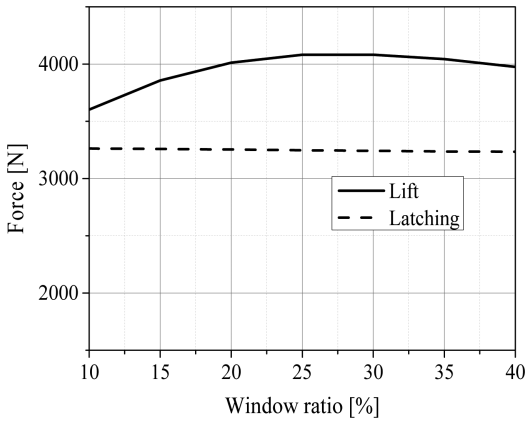

Fig. 9. Lift and latching forces from the third optimization step.

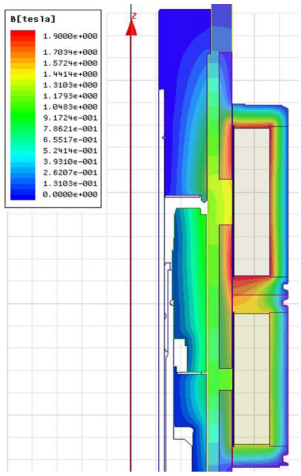

Fig. 10. (Color online) Flux lines and magnetic flux density distribution for the analysis case 5 of the third optimization step.

3) The third optimization step

CRDM lift and latching forces using the optimized latching window ratio from Step 2 and the varying lift window ratio were estimated, and the optimal design range of the lift window ratio was compared with the results

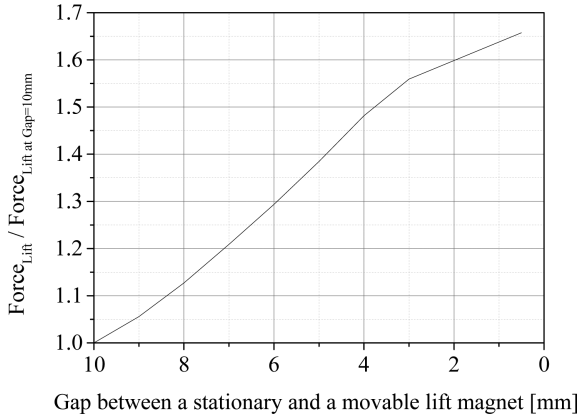

Fig. 11. Lift forces with respect to the gap approaching.

from Step 2. The lift window ratio changed from 10 % to 40 %. The distance from ⓐ in Figure 5 to the uppermost face of Flux ring A is assumed to be the same as the distance from ⓑ to the lowermost face. The latching window ratio was set to 16.5 % for convenience of the actual design. The analysis conditions and results are summarized in Table 4, and the estimated lift and latching forces are compared in Figure 9.

The results show that the lift force is maximized when the lift window ratio is about 25 % to 30 %, and this tendency coincides with the results from Step 1 and Step 2.

Case 5 seems to be the optimal design, and the flux lines and magnetic flux density distribution are shown in Figure 10 for this case. The lift and latching forces are 4,080 N and 3,240 N, respectively. The current SMART CRDM, which has a magnetic motor housing, can generate 4,100 N of the lift force, and thus it is estimated that there would be the 1.2 % loss of the lift force.

Because the results from Step 3 coincide with those from Step 2, it seems that there is no need to iterate the optimization process.

Figure 11 shows the lift force estimation results for Case 5 with respect to the gap approaching from 10 mm to 0.5 mm. As expected, after the sufficient lift force is generated between the stationary and movable lift magnets as an initial state of 10 mm gap, the lift force is getting increased with a smaller gap during the gap closing. Because the tendency is almost the same for all analysis cases, the non-dimensional forces are applied.

3. Design Effect of the Other Design Parameters

3.1. The effect of the magnetomotive force

The optimal design ranges for the lift coil and latching window ratio are different, at around 30 % and 15 %,

Table 5. Analysis results from magnetomotive force changes.

w_{lift}	w_{latch}	50 % MMF		200 % MMF	
$w_{lift\ coil}$ [N]	$w_{latch\ cc}$ [%]	F_{lift} [N]	F_{latch} [N]	F_{lift} [N]	F_{latch} [N]
5	16.5	1621.3	3180.4	4727.2	3299.3
10		1808.9	3163.2	5077.5	3298.5
15		1859.6	3155.8	5350.1	3296.9
20		1848.1	3154.9	5534.5	3296.9
25		1819.9	3153.6	5635.8	3293.3
30		1780.4	3155.3	5676.1	3291.0
35		1745.3	3153.8	5665.0	3291.4
40		1705.5	3154.3	5620.6	3287.8

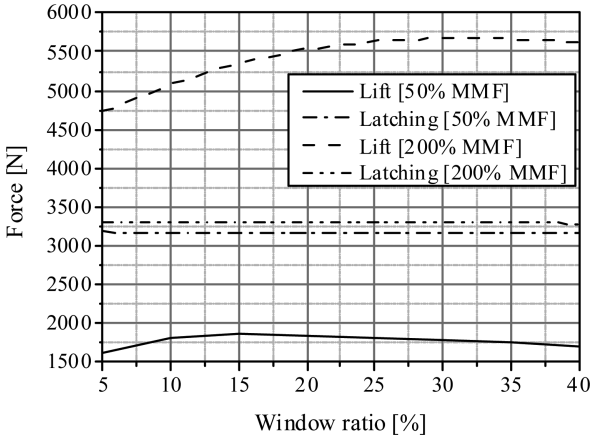

Fig. 12. Lift and latching forces according to the magnetomotive forces.

respectively. The main cause might be the difference in magnetomotive force (MMF); the MMF on the lift coil is about three-times greater than that on the latching coil. The effect of the MMF on the flux ring design was studied.

The latching window ratio is set at 16.5 %, and the lift window ratio varies from 5 to 40 %. The distance from ⓐ in Figure 5 to the uppermost face of Flux ring A, and the distance from ⓑ to the lowermost face are the same, as are the distances for Flux ring B.

Two lift coil MMFs were considered: 50 % and 200 % MMF of the current SMART CRDM lift coil. The analyses conditions and results are summarized in Table 5, and the estimated lift and latching forces are compared in Figure 12. The optimal window ratio is located at around 15 % for half of the MMF, and moves to around 30 % for double the MMF. Therefore, it can be concluded that the optimal window ratio is dominantly affected by the MMF.

3.2. The effect of the flux ring center position

The width center of the flux ring window was assumed to be aligned with the width center of the coil housing.

Table 6. Analysis results from flux ring center deviation.

Case	Window center deviation [mm]		F_{ligt} [N]	F_{latch} [N]
	Lift	Latching		
1	−10		3629.7	3241.2
2	−5		3894.3	3243.5
3	0		4080.4	3243.1
4	5	0	4199.0	3251.0
5	10		4199.0	3249.9
6	15		4096.4	3255.0
7	20		3874.8	3253.9

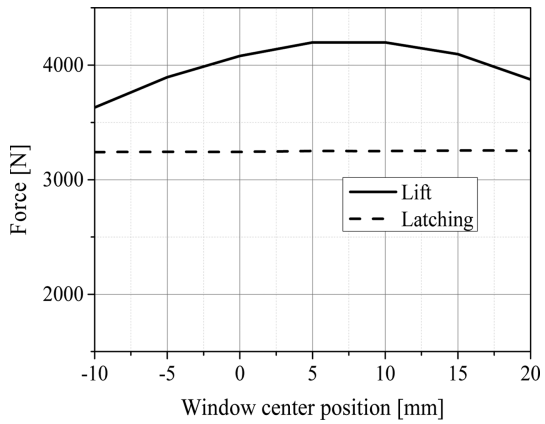

Fig. 13. Lift and latching forces according to flux ring center deviation.

The effect of the location of the width center of the flux ring window is studied. The window ratios are set to the optimal points from the previous study, and the MMFs are set to the current SMART CRDM operating condition. The width center of the lift coil flux ring window moves up (+) or down (−), and the corresponding lift and latching forces are estimated.

The analyses conditions and results are summarized in Table 6, and the estimated lift and latching forces are compared in Figure 13. The results show that the maximum lift force is generated when the window width center is located 5 to 10 mm above the coil width center. Only 3 % of the lift force increment is expected, so the design effect may be negligible.

4. Conclusion

The modified nonmagnetic motor housing with magnetic flux rings for the SMART CRDM was proposed and optimized through a finite element electromagnetic analysis by estimating the lift and latching forces. It was found that a nearly equivalent lift capacity would be achieved by the optimal housing and flux ring design, which will be proved experimentally. Because the optimal design point depends strongly on the magnetomotive force and there are two operating magnetomotive forces on each coil, the housing design will be optimized only for one operating condition at the final design stage. The same material as the coil housing for the flux rings was considered in the study; however, a magnetically excellent material such as Permendur or Hiperco may improve the magnetic transfer efficiency.

Acknowledgement

This work was supported by the National Research Foundation of Korea (NRF) grant funded by the Korea government (MSIP) (2016M2C6A1930040).

References

[1] A. Tanaka, K. Futahashi, K. Takanabe, C. Kurimura, J. Kato, and H. Hara, Int. J. Pres. Ves. Pip. **85**, 9 (2008).
[2] Westinghouse AP1000 DCD Section 3.9, NRC (2011).
[3] K. Takanabe, T. Miyake, and Y. Nagur, Nucl. Eng. Des. **214** (2002).
[4] Generic Design Assessment, Pre-Construction Safety Report, Sub-chapter 3.4, UK EPR
[5] KEPIC MI
[6] ASME Code Section XI
[7] K. Sawaragi, M. Taniguchi, Y. Tada, M. Kurokawa, and Y. Araki, Trans. ICONE (1999).
[8] V. Erguina and E. J. Kee, Trans. ICONE (2004).
[9] J. Lapena, M. d. S. Garcia-Redondo, F. J. Perosanz, A. Saez, D. Gomez-Briceno, and C. Castelao, Conference on Contribution of Materials Investigations and Operating Experience to LWRs' Safety, Performance and Reliability (2015).
[10] J. S. Park, H. M. Kim, and I. Y. Kim, Trans. KNS Spring Meeting (2006).
[11] J. S. Park, M. G. Lee, H. M. Kim, and I. Y. Kim, Trans. KNS Autumn Meeting (2009).
[12] J. S. Lee, H. G. Jun, and Y. J. Youn, IEEE Trans. Magn. **50**, 11 (2014).